The Quadrupole as a Source of Energetic Particles: II. The Static Equinoctal Cusp

[1]R. B. Sheldon, [2]J.-S. Chen, and [2]T. A. Fritz

Short title:

Abstract.

The recent discovery of energetic particles trapped in the cusp (CEP) in close association with diamagnetic cavities (CDC) strongly suggest a new location for particle acceleration. We use relativistically correct particle tracing in a Tsyganenko 96 equinoctal cusp to discover which particles are trapped, and estimate their quadrupole adiabatic invariants. By mapping these trapped particles into the dipole, we predict the spectra, pitchangle distribution, and spatial distributions which may result from such a high latitude source, and show that it is in many ways similar to the observations of outer radiation belt electron injections. We scale the mechanism to other magnetospheres and the heliosphere to demonstrate that it is consistent with observations over vast spatial and energy scales.

INTRODUCTION

In an earlier paper, [*Sheldon et al.*(2005)] (SCF1), we argued that a quadrupole trap could function as an accelerator, a cross between a dipole and Fermi-accelerator, possessing the best features of both. Alternatively, a quadrupole accelerator is a generalization of the well-known Fermi-I and Fermi-II acceleration mechanism, where the compressional energization goes into the perpendicular, rather than the parallel velocity. Since this was a novel mechanism, we argued in general terms for its significance at Earth, showing that it potentially could outperform both the dipole and bow-shock acceleration in terms of power and throughput.

In this paper, we present in more detail the way this physical mechanism may explain the somewhat mysterious origin of outer radiation belt electron (ORBE) injections [*McIlwain*(1996), e.g.,], and physically link them to solar wind conditions that impact the quadrupole cusp. This placement of source of MeV electrons outside the dipole but inside the magnetosphere may account for their recent discovery by POLAR [*Sheldon et al.*(1998a); *Chen et al.*(1997); *Chen et al.*(1998)]. Likewise, the physical mechanism we propose may also explain some of the peculiar correlations and non-linear relations observed between MeV injections and solar wind/magnetospheric activity [*Paulikas and Blake*(1979); *Baker et al.*(1986); *Koons and Gorney*(1991); *Li et al.*(2001)].

As we argued in SCF1, a trap is thermodynamically preferred for acceleration, both because the efficiency of energy conversion is higher for a multi-step, stochastic process, and because the total energy required for particle acceleration in minimized. Now a quiescent, static trap does not accelerate, that is a property of the trap dynamics. But in order to write the dynamics equations, the ground state of the static trap must be understood. That is, dynamics perturbs the Hamiltonian around an assumed equilibrium solution. Since the quadrupole accelerator is novel, this paper will not solve the dynamical problem, but will describe the static equilibrium solution.

Accordingly in section one, we discuss the particle tracing tools we used to find the volume of phase space trapped in the quadrupole. In section two, we map that phase space

volume to the dipole, and estimate some characteristic particle distributions to compare with data. In section three, we generalize the mechanism as best we can to other planetary magnetospheres, and compare with data, before concluding.

PARTICLE TRACING METHOD

We traced both protons and electrons through a quadrupolar cusp region of a T96 [*Tsyganenko and Stern*(1996)] magnetosphere for 093 Julian date in IGRF epoch year 2000 at 0000 UT, using a solar wind of 3/cc at 400 km/s and 10nT Bz north. Dst is a nominal +10 nT characteristic of an extended quiet period with little or no ring current. We calculated the center of the cusp to be at GSE coordinates (6.88, -0.04, 10.1) at a radius of 12.23 Re from the Earth.

Particles were given initial conditions at various perpendicular radii (0-6 Re), and at various parallel distances (-3 to 1 Re) from this central point at two different MLT ”sides” of the cusp, 0000 and 1200MLT. The program looped through a range of starting energies (200-1400 keV for electrons) and local pitchangles (70, 80, and 90 degrees), or five nested loops altogether.

For each starting location, provisional cusp invariants were calculated. The cusp magnetic moment is defined identically with the dipole, or perpendicular energy divided by magnetic field strength. The gyrophase for all particles was started at 0. The cusp second invariant should be calculated by integrating the parallel velocity along the bounce orbit, instead we used the proxy of the cusp equatorial pitch angle (CEqPA), or the pitchangle of the particle when it arrives at the high latitude minima on the gyrocenter field line. The bounce phase is the distance from the cusp equator along the fieldline, and was started from -3 Re to +1 Re. Finally, the third invariant is proportional to the flux enclosed by a drift orbit around the cusp, but without knowing whether the drift trajectory is closed, we cannot calculate this beforehand. So we use as a proxy the Euclidean distance from the fieldline minima to the quadrupole center (C-shell). The drift phase is the clock angle around the cusp (CLT), which

is relative to the quadrupole null rather than the Earth's surface field, with 1200 being in the plane that includes the sun and the B-field vector at the quadrupole null.

For these rigidity particles, the magnetic gradients are large, so that gyrocenter corrections must be made for the starting point, potentially violating all these invariants. In addition, the gyro-orbits can be quite large compared to the scale of the cusp. That is, we calculate the gyroradius for a given energy and starting position B-field strength, offset the field-line tracing to the gyrocenter and recalculate the first invariant. Given the large gradients, this is still only a first order correction, and near the quadrupole center, the higher order corrections may even diverge. When this happens, the particles are still traced, but the provisional invariants are set to zero.

Finally, we use a relativistically correct, ordinary differential equation solver [*Glasel et al.*(1999)] for the full equations of motion, based on Numerical Recipes [*Press et al.*(1986)] Bulirsch-Stoer routines as implemented at CERN. The ODE codes as well as the T96 codes are all in FORTRAN77 compiled with double precision. We use this method to avoid roundoff error in this stiff integration, with an accuracy much better than the Runge-Kutta 4/5 method used previously, e.g., [*Delcourt and Savaud*(1999)]. Failure to achieve highly accurate numerical integration leads to numerical diffusion in both space and invariants, which can cloud the results.

Despite our precautions, we discovered that truncation error in the magnetic field model was preventing us from drifting low-energy particles. Since the T96 model is a physical model of the magnetosphere, it is composed of multiple current systems all summed together vectorially, such as the paraboloidal Chapman-Ferraro current system, the cylindrical ring current, a 10th order IGRF internal multipole field etc. All these currents must add to zero in the region of the quadrupole center. Subtracting these large numbers results in less than three significant digits of magnetic field strength in the vicinity of the cusp corresponding to a scale length of about 10km. When the gyro-radius of the particles was smaller than about 100 km, this "posterizing" of the magnetic field caused the drift orbits to be erratic. So despite the real

improvement in adiabaticity for low energy particles, the numerical particle tracing showed a loss of the third adiabatic invariant.

We terminated the particle tracing if either the particle exceeded 160 minutes, 200,000 timesteps, or exited a GSE box ((0,20),(-12,12),(-1,20)). Although strictly speaking, the third quadrupole invariant is defined by a closed orbit around the cusp, we use a time threshold as a shortcut to estimate the presence of the third invariant.

Particle orbits are classified as chaotic, quasi-trapped, and well-trapped. For a trapped particle with cusp-equatorial pitchangles less than 90 degrees, one can observe all motions associated with the three invariants: gyration about a field line, bouncing along a field line around the off-equatorial minimum, and drift around the cusp. The sum of these motions produce the ”lily-shaped” orbits described by [*Sheldon et al.*(1998b)].

PHASE SPACE MAPPING

Using the three provisional invariants above with trapping time threshold $>$5980(1998) seconds, or a quasi-trapping threshold $>$980(198) seconds for protons(electrons) as a proxy for the existence of a third invariant, we can then classify the thousands of protons and electrons traced through the cusp as trapped (blue), quasi-trapped (red), or chaotic (green). Figure 1 shows the electrons, figure 2 shows the protons in a four panel projection of the 3-D phase space. In the lower left is a 3-axis projection, whereas the remaining panels show projections into two dimensions only. Note that the axes are arranged so that the three 2-D panels can be folded into the sides of a box.

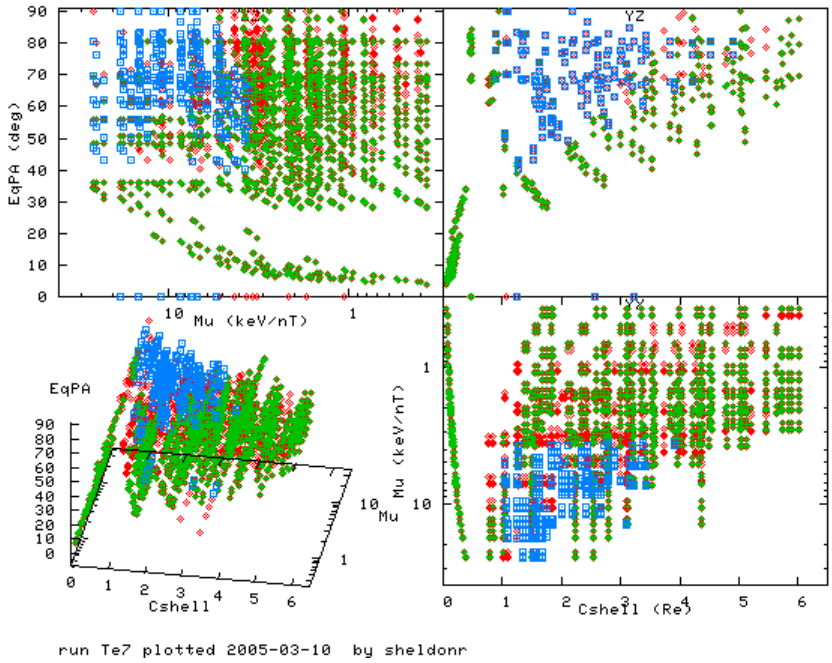

Figure 1. Electron phase space mapping. Green are chaotic, red are quasi-trapped, blue are trapped.

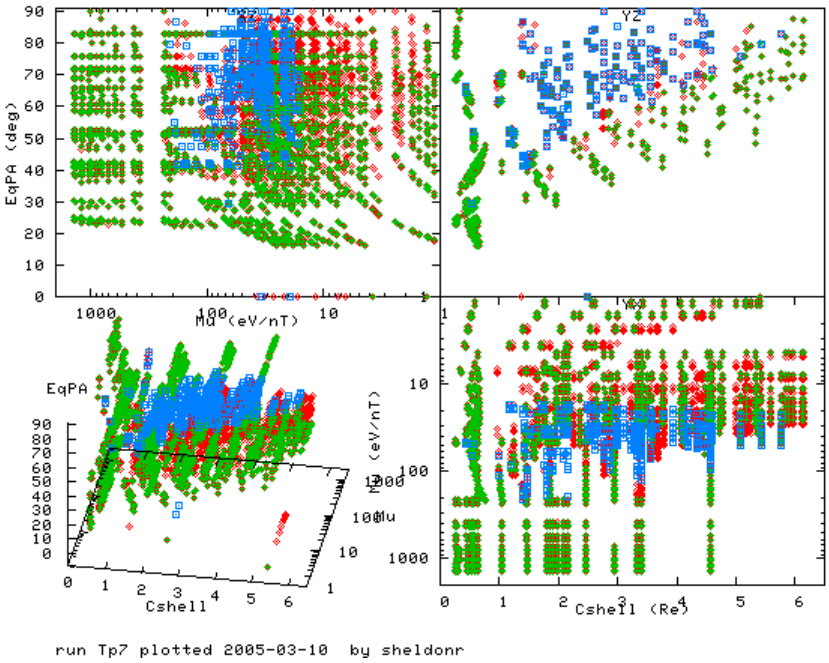

Figure 2. Proton phase space mapping. Green are chaotic, red are quasi-trapped, blue are trapped.

From the upper left panel for electrons in Fig 1, we see that the maximum magnetic moment trapped is about 25 keV/nT, and cusp equatorial pitchangles (EqPA) range from 40-90 degrees. The cutoff at 3 keV/nT between trapped and quasi-trapped (blue vs. red) we attribute to numerical roundoff errors in the magnetic field model, which would be trapped if a better numerical field model were used.

The upper right panel shows that the C-shell varies from 1-5 Re, with a high threshold that depends on CEqPA, larger for locally 90 degree pitchangles. The absence of trapping below C-shell$\sim$1 we attribute to the very small $|B|$ near the center which destroys the invariants. Note the number of quasi-trapped orbits at large C-shell, which we attribute to

the CLT asymmetry of the quadrupole cusp causing some electrons to escape before they complete a drift orbit.

Finally, the bottom right panel shows a similar quasi-linear dependence of the high C-shell with magnetic moment, larger for smaller magnetic moment. We recognize the same 3 keV/nT numerical limit seen in the left panel. Reference to the lower left panel, shows that the trapped (blue) points form a compact cloud surrounded by untrapped or quasi-trapped orbits, demonstrating that phase space is well-ordered, that trapping is truly occurring.

Similarly for the protons in Fig 2, the same compact cloud of trapped electrons is seen in phase space, however, the scale for magnetic moment has changed, ranging from 1-1000 eV/nT. The maximum limit is at 200 eV/nT and threshold for numeric roundoff occurs at 15 eV/nT, but otherwise the trapping regions for both are remarkably similar. This tells us that the primary difference between relativistic electrons and warm protons is their gyro-radii. Once this is accounted for, the two trapped particle distributions are nearly identical.

We must point out, however, that our simulation has no electric field. Should there exist even as little as 1 mV/m field, the proton drift orbits would be greatly distorted, whereas the relativistic electrons would hardly notice. The effect of this distortion would be to shrink the volume of the proton trapping region, making the cusp into an asymmetric trap and possibly a source of space charge as well.

Now if these trapped particles pitchangle scatter, they will not change their energy, but they will reduce their magnetic moment and simultaneously lose their 2nd quadrupole invariant. That is, they will escape the high-latitude minima and travel along the magnetic field line toward the dipole equator. Depending on their CLT, this field line could be on the dayside, around the flanks or down the tail. Alternatively, the particle can betatron energize due to a cusp compression, and exceed the trapping limit in magnetic moment or Cshell. Once again, the escaping particle will appear at the dipole equator, but with much the same magnetic moment as before.

Therefore mapping the magnetic moments from the cusp to the dipole gives a upper

limit 0.2(25) keV/nT for protons(electrons), which around L=5 Re or 240 nT corresponds to 48(6000) keV particles. That is, the peak energy of the ion ring current, and the peak energy of the outer radiation belt electrons (ORBE) both map to the magnetic moment upper limit of the cusp trapping region.

Since the $|B|$ minima in the cusp can be deeper or shallower than the corresponding dipole equator, the dipole equatorial pitchangle of the escaping particles varies between ¡40-90 degrees, with a probable peak away from 90 degrees. In the outer dipole magnetosphere, or in the tail, the equatorial field strength can often be smaller than that of the 1-6 Re C-shell region, which excludes the near 90 deg pitchangles. The near 0 deg pitchangles are also excluded because of the wider ”loss cones” of the cusp trapped population. As a consequence, the escaping pitchangle distributions (PAD) will appear as ”butterfly” PAD, especially in the outer magnetosphere. Subsequent diffusion into the inner dipole magnetosphere would tend to drive these butterfly PAD toward a 90 deg peaked or ”pancake” PAD, but residues of the butterfly distribution might be discernible as ”head-and-shoulder” PAD [*Sheldon*(1990); *Sheldon and Hamilton*(1993)].

Finally the cusp trap does not map to the entire dipole, it only has access to the outer regions of the dipole. The smallest dipole L-shell which threads through the cusp trap occurs at noon, and determines the minimum L-shell boundary for cusp particle ”injections” into the dipole. It depends on the topology of the cusp, which varies with UT, but for the equinoctal cusp this minimum L-shell will be at its maximum value. That is, the solstices would have deeper penetration of cusp injections.

OTHER MAGNETOSPHERES

Since these trapping limits in the quadrupole cusp appear to depend only on rigidity of the particles, we argue that the topology of the cusp is the most important controlling factor. Accordingly, all dipole magnetospheres embedded in the solar wind will have a quadrupole trap whose geometry is determined by scaling the solar wind and planetary

magnetic field appropriately. Therefore using simple scaling arguments, we can estimate the ORBE population at all the measured magnetospheres, from Mercury to Neptune, and compare it to observations. This is a test whether the quadrupole cusp can be generalized or scaled, and whether it remains the most efficient accelerator after scaling. To our knowledge, it also the only such generalized theory of ORBE formation in comparative magnetospheres.

The scaling we need, then, is the size of the cusp, the magnetic field of the cusp, and the ratio of the cusp to planetary field strength. The first two items give us the rigidity of the maximum trapped particle, and the last item gives us the adiabatic energy increase of such a dipole injected cusp particle.

Since the rigidity or gyroradius determines the limiting magnetic moment, we have,

$$\rho \propto mv/qB_{CUSP} \ \text{or} E \propto B_{CUSP}^2 \rho^2 \tag{1}$$

Now it is clear that the gyroradius must be smaller than the radius of the quadrupole cusp, which in turn is some fraction of the distance to the stagnation point, so we can write $\rho \propto rkR_{STAG}$, where k is some conversion from stagnation distance to cusp size, and r is the planetary radii in meters. Substituting the dipole approximation, $B_{CUSP} = B_0/R_{STAG}^3$, where B_0 is the surface field, and R_{STAG} is the distance from the planet to the subsolar stagnation point of the magnetosphere in planetary radii, we have

$$E \propto (B_0 rk)^2/R_{STAG}^4 \tag{2}$$

Taking the ratio with Earth radiation belts eliminates all the constants in common, giving

$$\frac{E_{PLANET}}{E_{EARTH}} = \left(\frac{B_0}{B_{EARTH}}\frac{Rp}{Re}\right)^2 \left(\frac{R_{EARTH}}{R_{STAG}}\right)^4 \tag{3}$$

Normalizing to 5 MeV for the radiation belts at Earth, gives the following table:

Table 1. ORBE Scaled to Earth

Planet	R_STAG Planet r	Rp/Re	B_0 nT	E_RAD keV	Obs. keV	Pred./Obs.
Mercury	1.4	0.38	330	660	45	14
Venus	1.1	0.95	<10	<4	–	–
Earth	10.4	1.00	31,000	5000	n/a	n/a
Mars	1.25	0.53	<6	<0.5	–	–
Jupiter	65	11.2	430,000	7100	100000	1/14
Saturn	20	9.5	21,000	1600		
Uranus	20	4.0	23,000	810		
Neptune	25	3.8	14,000	120		

Note that the table predicts a 7 MeV radiation belt at Jupiter, which is about 1/10 of the observed energy peak, which might be attributed to the inflated dipole at Jupiter leading to anomalously large cusp and cusp fields. The large value at Mercury is also somewhat surprising, but possibly consistent with the Mariner data if the instrument were functioning without pulse pileup [*Christon*(1987); *Christon*(1989)]. Otherwise the simple scaling has all the right features, strong belts at Jupiter, moderate belts at the outer planets, weak or nonexistent at the inner planets.

Since the Sun is also magnetized and embedded in the flowing inter-stellar medium (IMF), we might also expect a some cusp acceleration. However the topology is considerably different, so we have to set up a radically different picture. The fact that the Sun's dipole is tilted with respect to its rotation axis, means that the solar wind carries with it a $27/2 = 13$ day polarity reversal separated by a current sheet. Since the field spirals out like a water sprinkler, (a Parker, or more correctly, an Archimedean spiral) by the time the field has reached the heliopause it is nearly perfectly tangential. This results in a marble cake appearance as the field reverses tangential direction every 13 days. The thickness of this layer is approximately $13d * 24hr/d * 3600s/hr * 400km/s = 3AU$, but due to compression at the heliopause, thins

down to ∼1 AU.

From SCF1, we argued that cusp acceleration was a generalization of Fermi acceleration to the perpendicular component. This is precisely what appears to be happening to the plasma, which is trapped in tangential layers undergoing compression. However it is not first order, but second order acceleration that concerns us, which is the heating due to random fluctuations in the compression. So the particles must circulate around the B-field within the layer, giving a gyroradius of about 0.5 AU. Meanwhile the magnetic field has decreased by 1/R from its Earth value of, say, 5nT at 1 AU to 0.05 nT at 100AU. Again, the compression raises that value by a factor 4, giving 0.2 nT in this compressed layer. Plugging these constraints into a rigidity calculation gives:

$$\rho = p_{\perp}/(qB) \tag{4}$$

$$\gamma = \left(1 + \left(\frac{\rho q B}{mc}\right)^2\right)^{1/2} \tag{5}$$

$$K = (\gamma - 1)mc^2 \tag{6}$$

which is relativistically correct.

Assuming that galactic cosmic rays appear in this region fully stripped, and that anomalous cosmic rays (ACR) are only singly charged, we calculate the following high-energy cutoffs, which would appear as a peak in the energy spectrum right below the cutoff. Many features of this model are similar to standard ACR acceleration theory, which invokes diffusive transport in the presence of Corotationg Interaction Region (CIR) shocks. In contrast, we use adiabatic transport (not diffusive) which can be trapped in a current layer (rather than shocks). This also permits the acceleration to occur in thinner layers, rather than the more global CIR structures. Of course, the standard theory is far more developed with much better predictions. Our question is whether the acceleration theory we have developed can be fruitfully applied to the heliopause.

Table 2. Cosmic Rays at the Heliopause

Specie	Charge	ρ	B	K	K/nuc
	e	AU	nT	MeV	MeV/nuc
electron	-1	0.3	0.2	2690	—
Galactic H	1	0.3	0.2	1900	1900
Galactic He	2	0.3	0.2	2790	700
Galactic O	8	0.3	0.2	11100	700
Anomalous H	1	0.3	0.2	1900	1900
Anomalous He	1	0.3	0.2	860	215
Anomalous O	1	0.3	0.2	238	15

From the table, it can be seen that the model correctly predicts the peak in both the galactic protons and electrons. Jokipii argues that the cutoff for ACR He is at ∼60 MeV/nuc, and ACR O is at ∼15 MeV/nuc. We seem to do well for O, but overpredict the ACR He peak by a factor of 3.

CONCLUSIONS

The agreement at Earth is striking, with ORBE injections having many of the same properties as our theoretical cusp injections: 5 MeV energy inner L-shell penetration limit, butterfly PAD, and equinox to solstice asymmetry. In this work we have calculated static properties of the phase space volume, but the dynamics of ORBE injections are also very encouraging for future work. Intriguingly, the cusp protons were found to map nicely to the ring current, suggesting that the near Earth plasma sheet may not be the only source of ring current injections. However, realistic electric fields will strongly impact the cusp protons, and must be taken into account in future models.

The comparison with other magnetospheres is another test of the mechanism, for which the scaling model performed modestly well. It may have overpredicted Mercury

while underpredicting Jupiter. These effects may be due to unique features of these two magnetospheres, with Mercury occupying a larger fraction of the magnetospheric volume than any other planet, and Jupiter inflating its magnetosphere with Io plasma, departing quite substantially from a dipolar field.

The comparison to ACR acceleration showed that the model could correctly predict aspects of this well-known phenomena. Without claiming superiority, our model may perhaps provide a complementary source of ACR in the current simulations.

Three different tests of the mechanism were examined, and while high accuracy was not obtained, order of magnitude agreement suggests that the mechanism has not been invalidated by any of the data.

Acknowlegements

We acknowlege fruitful conversations with colleagues at NASA/MSFC/NSSTC and NASA grants NAG-5 2578, NAG-5 7677, and NAG-5 1197 at Boston University.

References

Baker, D. N., J. B. Blake, R. W. Klebesadel, and P. R. Higbie. Highly relativistic electrons in the earth's outer magnetosphere 1. lifetimes and temporal history 1979–1984. *J. Geophys. Res.*, *91*, 4265–4276, 1986.

Chen, J., T. A. Fritz, R. B. Sheldon, H. E. Spence, W. N. Spjeldvik, J. F. Fennell, and S. Livi. A new temporarily confined population in the polar cap. *Geophys. Res. Lett.*, *24*, 1447–1450, 1997.

Chen, J., T. A. Fritz, R. B. Sheldon, H. E. Spence, W. N. Spjeldvik, J. F. Fennell, S. Livi, C. Russell, and D. Gurnett. Cusp energetic particle events: Implications for a major acceleration region of the magnetosphere. *J. Geophys. Res.*, *103*, 69–78, 1998.

Christon, S. P. A comparison of the mercury and earth magnetospheres: Electron measurements and substorm timescales. *Icarus*, *71*(3), 448, 1987.

Christon, S. P. Plasma and energetic electron flux variations in the mercury 1 c event: Evidence for a magnetopause boundary layer. *J. Geophys. Res.*, page 6481, 1989.

Delcourt, D. C. and J. A. Savaud. Populating of the cusp and boundary layers by energetic (hundreds of kev) equatorial particles. *J. Geophys. Res.*, *104*, 22,635, 1999.

Glasel, J., J. D. Sullivan, and T. A. Fritz. *EOS Trans. Suppl.*, *SM32D-10 S283*, 1999.

Koons, H. C. and D. J. Gorney. A neural network model of the relativistic electron flux at geosynchronous orbit. *J. Geophys. Res.*, *96*, 5549–5556, 1991.

Li, X., M. Temerin, D. Baker, G. Reeves, and D. Larson. Quantitative prediction of radiation belt electrons at geosynchronous orbit based on solar wind measurements. *Geophys. Res. Lett.*, *28*, 1887, 2001.

McIlwain, C. E. Processes acting upon outer zone electrons. In J. F. Lemaire et. al, editor, *Radiation Belts Models and Standards*, Washington DC, 1996. AGU.

Paulikas, G. A. and J. B. Blake. Effects of the solar wind on magnetospheric dynamics: Energetic electrons at geosynchronous orbit. In W. P. Olson, editor, *Quantitative Modelling of Magnetospheric Processes, Geophys. Monogr. Ser.*, volume 21, page 180, Washington, D.C., 1979. AGU.

Press, W. H., S. A. Teukolsky, W. T. Vetterling, and B. P. Flannery. *Numerical Recipes: The art of scientific computing*. Cambridge Univ. Press, Cambridge, 1986.

Sheldon, R. B. and D. C. Hamilton. Ion transport and loss in the earth's quiet ring current 1. data and standard model. *J. Geophys. Res., 98*, 13,491–13,508, 1993.

Sheldon, R. B., H. E. Spence, and J. F. Fennell. Observation of 40 kev field-aligned ion beams. *Geophys. Res. Lett.*, *25*, 1617–1620, 1998a.

Sheldon, R. B., H. E. Spence, J. D. Sullivan, T. A. Fritz, and Jiasheng Chen. The discovery of trapped energetic electrons in the outer cusp. *Geophys. Res. Lett.*, *25*, 1825–1828, 1998b.

Sheldon, R. B., T. A. Fritz, and J.-S. Chen. The quadrupole cusp as the source of cusp energetic particles: I. general considerations. In *AGU*, 2005. submitted to AGU Monograph Series.

Sheldon, R. B. *Ion transport and loss in the quiet terrestrial ring current*. PhD thesis, University of Maryland, College Park, MD, 1990.

Tsyganenko, N. A. and D. P. Stern. Modeling the global magnetic field of the large-scale Birkeland current systems. *J. Geophys. Res.*, *101*, 27187–27198, 1996.

Received _____